The Corrosion Behavior of TiN Coated and Uncoated Incoloy 800 Alloy

B.S. Yilbas, M.M. Khaled, R. Kahraman, A. Qutub, Z. Khan, B.J. Abdulaleem, and M. Ouerfelli

(Submitted 9 March 1998; in revised form 29 May 1998)

Incoloy alloy 800 is used in a variety of applications in industry as well as in domestic appliances for sheeting on electric heating elements. The composition of the alloy enables it to resist deterioration in many corrosive environments. However, resistance of the alloy to corrosion in aqueous media needs to be further examined. The present study examines the corrosion properties of Incoloy 800 alloy of both coated and uncoated workpieces obtained in a 0.1N H_2SO_4 + 0.05N NaCl solution. TiN coating is achieved using a physical vapor deposition (PVD) technique while corrosion tests are carried out using electrochemical polarization methods. Moreover, in order to examine the influence of hydrogen diffusion, reduction of hydrogen at the Incoloy 800 surface is carried out in a solution of 0.1N HNO_3 + 1 g/L thiourea. Tensile tests are conducted on the workpieces to determine the influence of hydrogen embrittlement on the resulting mechanical properties of the substrate. To examine the pit formation and stress induced microcracking, scanning electron microscope (SEM) analysis is carried out. The results show that the corrosion resistance of the alloy improves after TiN coating. In addition, no specific pattern or differentiation on the pit geometry is observed. The pitting rate and its size reduce considerably for TiN coated workpieces.

Keywords alloy 800, corrosion, pitting, TiN coating

1. Introduction

Incoloy alloy is widely used in a variety of applications involving exposure to corrosive environments. It is also used as a material for construction of equipment that should resist oxidation, carburization, and other effects of high temperature exposure. The high percentage of nickel maintains an austenitic structure so that the alloy is ductile. The nickel content contributes resistance to scaling, corrosion, and stress-corrosion cracking (SCC). Moreover, the iron content provides resistance to internal oxidation.

The influence of thermal processing on the corrosion resistance of nickel-base alloys in sour gas environments was investigated by Moeller (Ref 1). He considered the reduction of cost of corrosion-resistant tubing by using less expensive materials. The analysis of diffusion-controlled release of hydrogen from nickel and Inconel 600 was investigated by Shewmon et al. (Ref 2). They indicated that highly strained regions contained almost ten times the hydrogen trapped in the unstrained regions. Electrochemical and SCC behavior of nickel-base alloy was investigated by Tsai et al. (Ref 3). They determined the crack propagation velocities and developed a functional relation for SCC grow rate.

Since the discovery of the pitting of nickel alloy tubing in service, some research was conducted to determine its causes (Ref 4). Although some progress has been made in determining the causes of pit initiation and pit growth, less attention has been focused on the subject of pit propagation in nickel alloys. However, shallow pitting was found on nickel alloy heated tubing tested with in-leakage of seawater (Ref 5). King and Doutovich (Ref 6) investigated the pitting process on the long-term exposure and they showed that relatively deep pits occurred in external tube surfaces. Isoacs (Ref 7) conducted a program for nickel alloy to determine the kinetics of pit initiation and growth by monitoring the electrochemical potential and current flow at room temperature range. They showed that as chloride concentration and temperature increased, the electrochemical potential decreased; therefore, it was suggested that the pitting initiated more readily at the higher temperature and at the higher chloride concentration.

In the present study, the corrosion behavior and hydrogen embrittlement of Incoloy 800 alloy are investigated. To investigate

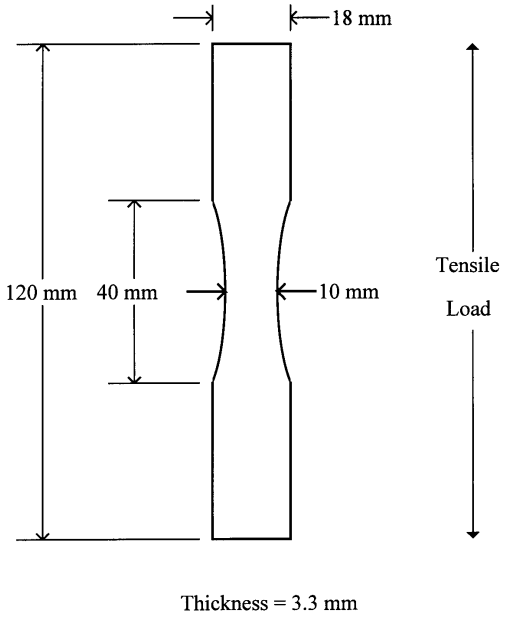

Fig. 1 Tensile test specimen

B.S. Yilbas, **A. Qutub, Z. Khan, B.J. Abdulaleem,** and **M. Ouerfelli,** Department of Mechanical Engineering; **M.M. Khaled,** Department of Chemistry; and **R. Kahraman,** Department of Chemical Engineering, King Fahd University of Petroleum and Minerals, Dhahran 31261, Saudi Arabia.

formation of pitting and the corrosion process, both TiN coated and uncoated workpieces are considered. Tafel and linear polarization experiments are conducted for both workpieces to measure the corrosion resistance of the substrates. The influence of the hydrogen diffusion on the mechanical properties of the alloy is also investigated. After the completion of the electrochemical tests, the tensile test is conducted to determine the effect of hydrogen embrittlement on the mechanical properties of the alloy. SEM is conducted to explore the pits and cracks developed in the workpiece surface vicinity.

2. Experiment

TiN coating was carried out using a PVD technique. Incoloy 800 workpieces were ground, polished, and ultrasonically cleaned. A PVD unit operating with a direct current magnetron source was used. The workpiece material was held at 260 °C in the coating unit. After the titanium sputtering, N^+ ions were implanted at an acceleration potential of 50 keV. A series was formed of nominal constant-thickness single layers of 400 nm film. Consequently, with multi-pass, the total thickness of the multilayer film of about 2 μm was formed on the surface of the substrate.

The coated and uncoated workpieces were degreased in acetone and benzene before conducting the electrochemical tests, in which 0.1N H_2SO_4 + 0.05N NaCl was used as a solution. However, for the hydrogen diffusion process, a solution of 0.1N HNO_3 + 1 g/L thiourea was used. The electrochemical experiments were performed using an EG&G PARC model 273 A Potentiostat-Galvanostat. The electrochemical cell was a three-electrode cell. An Ag/AgCl electrode was used as a reference electrode. The working electrode was the Incoloy 800 electrode. A platinum electrode of 1 cm^2 was used as an auxiliary electrode. Tafel and linear polarization experiments were conducted to determine the corrosion rates of the coated and uncoated workpieces.

Tensile tests for workpieces subjected to the electrochemical test and untreated were carried out using Instron 1196 mechanical testing equipment. SEM analysis of the workpiece surfaces and their cross sections was carried out after the electrochemical and tensile tests. Figure 1 shows the size of the specimen and the direction of tensile forces applied, while Table 1 gives the elemental composition of Incoloy 800 alloy.

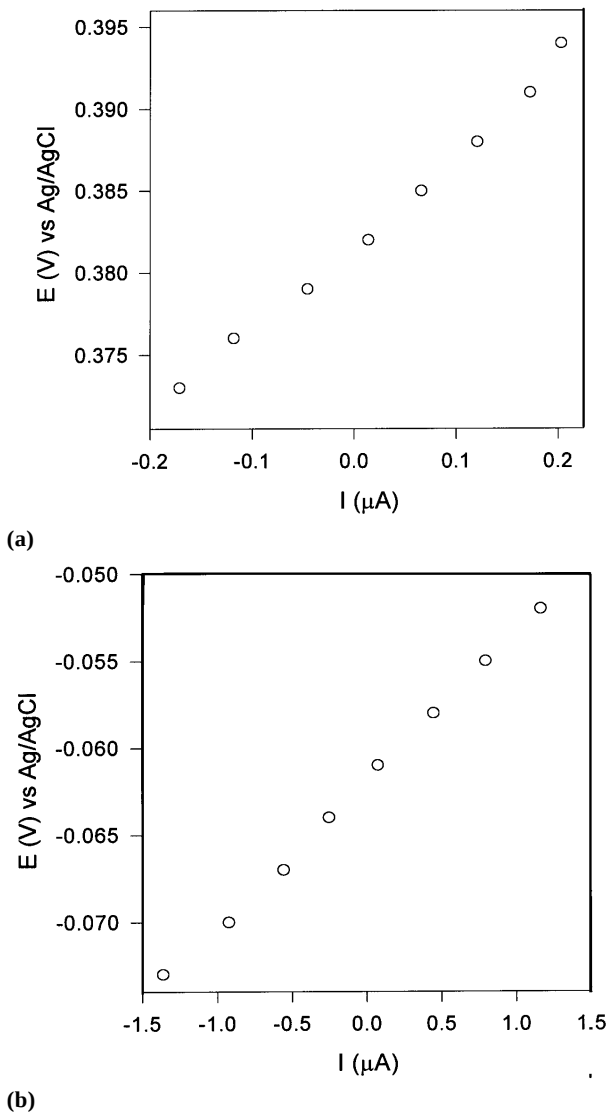

Fig. 2 Linear polarization of Incoloy 800 in 0.1 N H_2SO_4 and 0.05 M NaCl at scan rate of 0.166 mV/s. (a) TiN coated. (b) Uncoated

Table 1 Elemental composition of Incoloy 800 alloy

Component	Composition, wt%
Ni	30-35
Cr	19-23
Fe	39.5 min
C	0.1 max
Mn	1.5 max
S	0.015 max
Si	1 max
Cu	0.75 max
Al	0.15-0.6
Ti	0.15-0.6

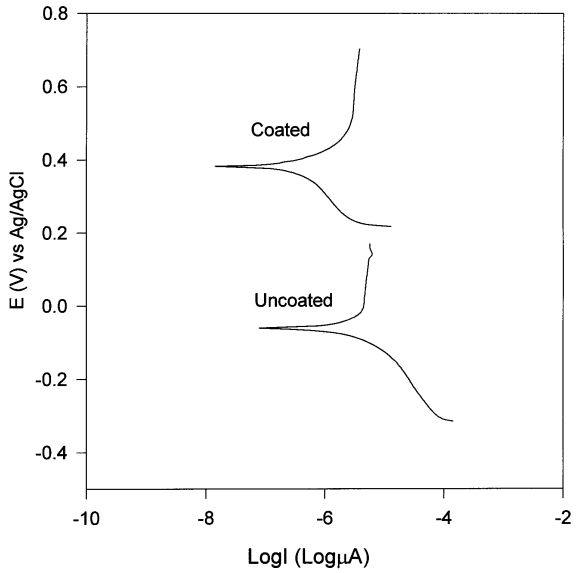

Fig. 3 Tafel plots of Incoloy 800 in 0.1 N H_2SO_4 and 0.05 M NaCl at scan rate of 1mV/s.

3. Results and Discussions

The Tafel polarization curves for TiN coated and uncoated workpieces obtained in 0.1N H_2SO_4 + 0.05N NaCl aqueous solution are shown in Fig. 2. It is noted that the corrosion potential for the coated specimen is about 440 mV more noble than that of the uncoated one (Table 2). The uncoated workpiece results in a higher corrosion current than the TiN coated workpiece. However, disintegration of the sample surface was evident when an anodic current of 100 mA/cm^2 was applied for 2 h.

Figure 3 shows the linear polarization curve for TiN coated and uncoated workpieces. The corrosion current density for a TiN coated workpiece is about 30% less than that for the uncoated workpiece. Table 2 summarizes the Tafel and polarization resistance results. The coated sample results in minimum corrosion rate (about 11% of the corrosion rate of the uncoated specimen), and this may be attributed to a lesser number of coating defects, such as pinholes and cracks. However, some defects in the TiN coat are observed locally (Fig. 4). These pinholes are very small and narrow. The influence of pinholes on corrosion rate may not be significant, since the reaction rate is expected to be low in the narrow holes due to reduced mass transport between the bottom of the pinhole and the corrosive environment. Moreover, a local oxide formation is evident between the TiN coat and the base material (Fig. 4). In this case, this oxide film becomes chemically passive, which in turn increases the corrosion resistance of the substrate.

Figure 5 shows the cross sections of the pitted surfaces. It should be noted that the pitting is a form of localized attack leading to the loss of structural integrity of the component. In general, pitting is a two-stage process involving initiation and growth, followed perhaps by repassivation of the existing pits (Ref 8).

Examining the workpiece surfaces using SEM, the pit morphology can be obtained, which in turn gives the qualitative analysis of the corrosion product. It is expected that the corrosion products in pits are being enriched in chromium and depleted in nickel and iron (Ref 9). It should be noted that the amount of corrosion product inside the pits is an important factor controlling pit growth kinetics. In this case, the surface ion affects the formation of the corrosion product inside the pits. Also, the corrosion products are generally found on the workpiece surface (Fig. 5a). In all cases, the corrosion products are enriched in chromium and depleted in nickel and iron. In general, the morphology at the pit bottom consists of intergranular attack and secondary micropits (Fig. 5b). No specific pattern or differentiation on the pit geometry is observed. In all cases, lesser amounts of deposit are observed. This might suggest that the higher chromium content in the alloy decreases the amount of precipitation in the pit environment. The increase in pit width has the same pattern as that of pit depth. The observed aspect ratios varied from 0.25 to 0.36. However, some of the pits show significant lateral growth along the surface (Fig. 5c). Since saturation in pit growth occurs after some time, the secondary micropits may play an important role in the reactivation of the corrosion process. In general, removal of the pit deposit seems to yield a slightly high pit depth-to-width ratio. This may support the view that less pit deposit correlates with a low pit depth-to-width ratio. This may be due to the fact that more corrosion product within a pit affects the dissolution kinetics of the inner pit surface by increasing ohmic resistance.

Table 2 Corrosion rates of TiN coated and uncoated Incoloy 800 deduced from Tafel slopes and linear polarization experiments

Incoloy 800 specimen	E (I = 0), mV	Cathodic Tafel, V	Anodic Tafel, V	Corrosion current, μA	Polarization resistance, KΩ	Corrosion rate, mm/year
Coated	382	2.15	0.186	1.41	54.1	0.0347
Uncoated	–61	0.228	1.52	2.00	3.65	0.304

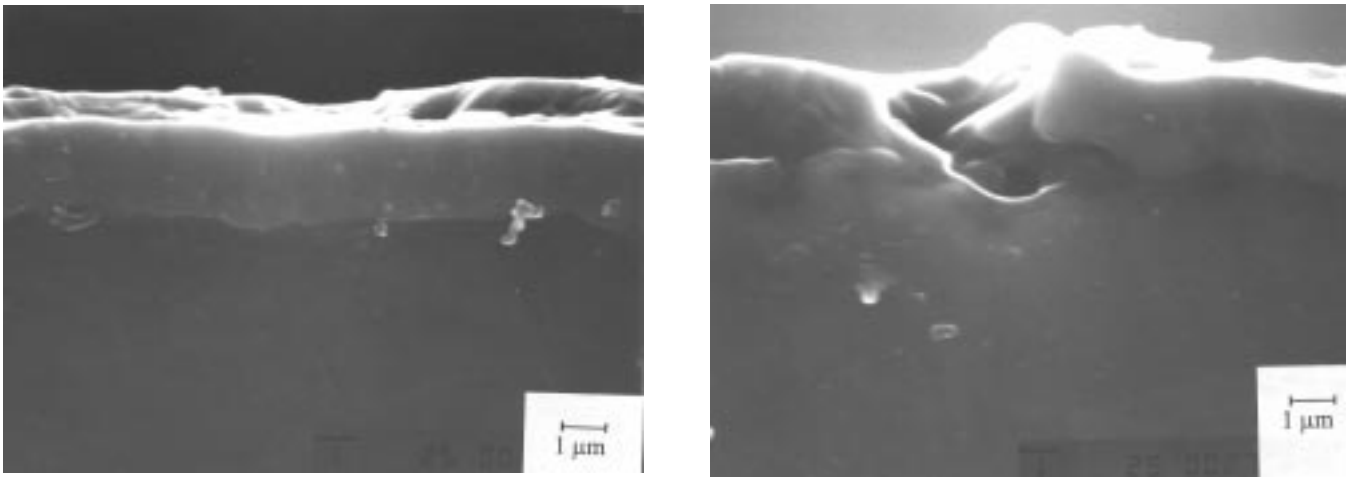

(a) **(b)**

Fig. 4 Photographs of (a) the cross section of TiN coated workpiece and (b) a pinhole formed in the TiN coat

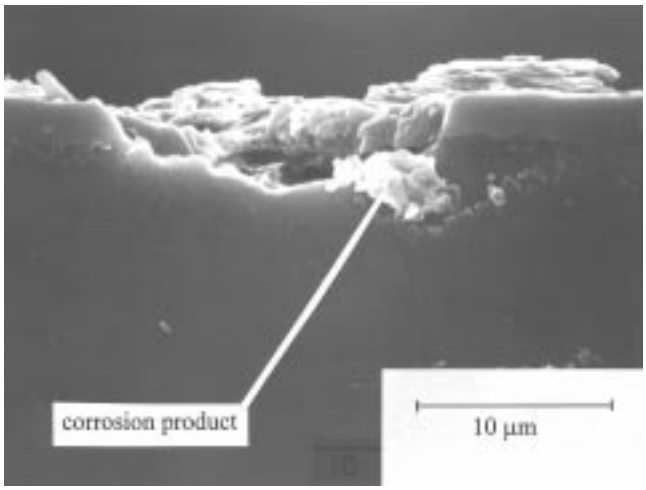

(a)

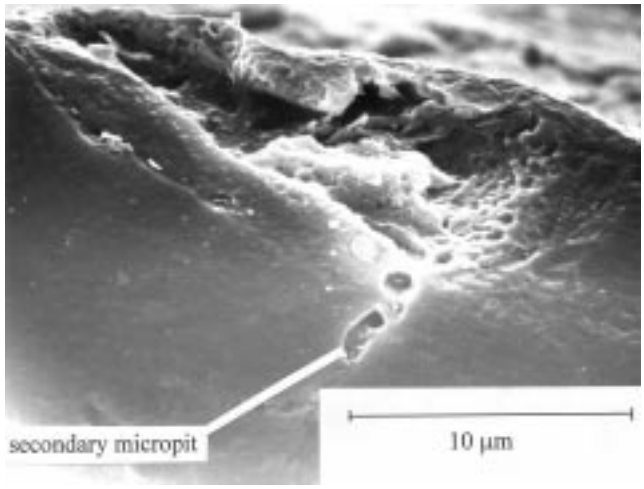

(b)

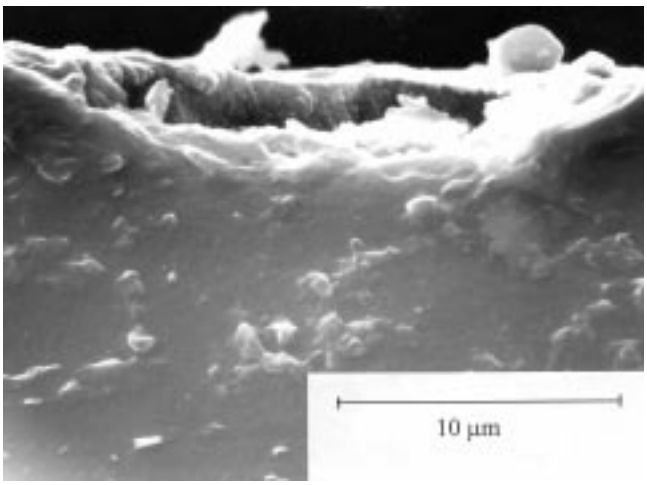

(c)

Fig. 5 Photographs of cross sections of pits formed in (a) a TiN coated workpiece, (b) an uncoated workpiece, and (c) an uncoated workpiece for which the pit is elongated laterally

Based on the pit depths observed, the amount of pit deposit and secondary pits seems to be associated with the reaction of a pit being repassivated, which leads to deeper pits. Removal of the corrosion product inside pits yields slightly narrow pits.

Figure 6 shows the tensile properties of both TiN coated and uncoated workpieces before and after hydrogen diffusion tests. The workpieces are not sensitive to hydrogen embrittlement, which occurs at the surface, since the mechanical responses of treated and untreated workpieces are similar. Moreover, after tensile testing the cross section close to the fracture surfaces is examined by SEM. The general aspect of cracking is intergranular, as shown in Fig. 7(a). The grain boundaries appear smooth and do not exhibit any strong traces of dissolution (Fig. 7b). Nevertheless, a detailed observation at a finer scale shows that even if the cracking is mostly intergranular, numerous grain boundaries exhibit microfacets, which correspond to a brittle decohesion.

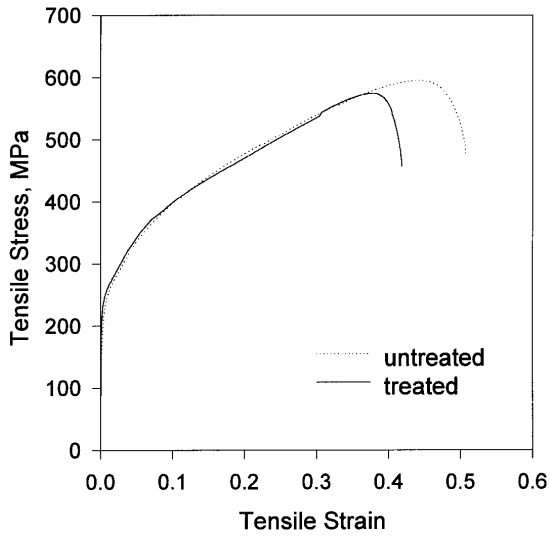

(a)

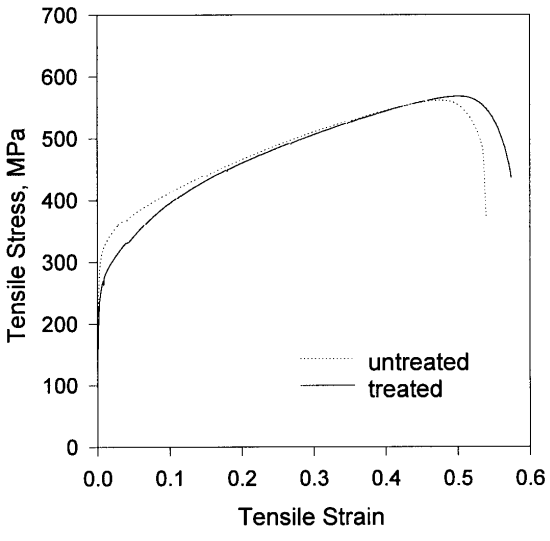

(b)

Fig. 6 Tensile stress versus strain plot for (a) uncoated and (b) TiN coated workpieces before and after electrochemical treatment

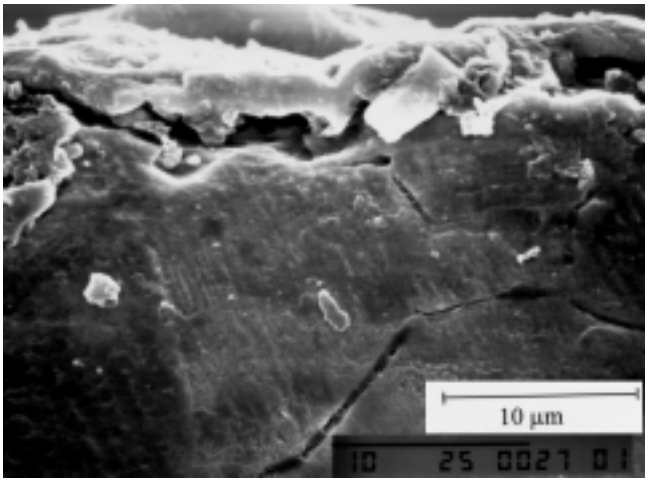

(a)

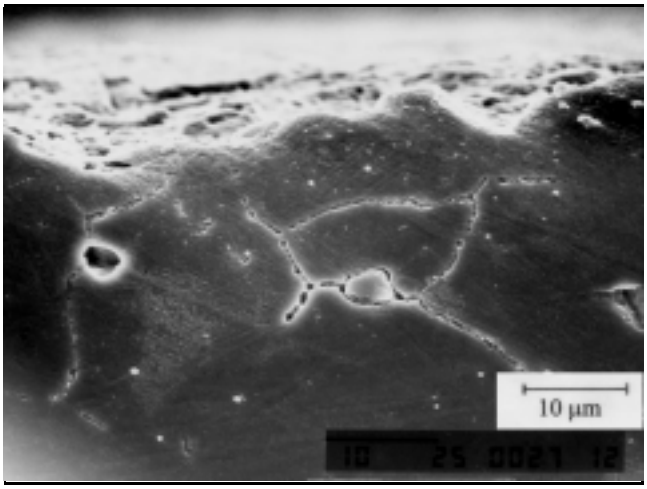

(b)

Fig. 7 (a) A photograph of a workpiece cross section, in which the intergranular cracking is visible. (b) A photograph of a workpiece cross section showing intergranular cracks

4. Conclusions

The Tafel and polarization test results show that the TiN coated workpiece results in considerably high corrosion resistance compared to uncoated samples. Few local coating defects do not appear to influence the corrosion resistance of the substrate significantly. Diffusion rate of the corrosive environment is believed to be low in the narrow pinholes formed in the coat. In addition, the local oxide layer formed between the coat and the base material chemically passivates the substrate, which in turn decreases the corrosion rate.

It may be seen from the morphology of the pitting sites that the pit bottom consists of intergranular and secondary micropits. However, no specific pattern or differentiation on the pit geometry is observed. Moreover, the lesser amounts of deposit are seen; in this case, the higher chromium content in the alloy reduces the corrosion reaction in the pit environment. The secondary micropits appearing at the bottom of the pit result in deeper pits, and this may become important in the reactivation process. The surface ion affects the formation of the corrosion product inside the pits, and the corrosion products are enriched in chromium and depleted in nickel and iron.

The workpieces with and without TiN coat are insensitive to hydrogen embrittlement occurring at the surface. The intergranular cracking is observed in the surface vicinity, and the grain boundaries appear smooth without any trace of dissolution.

Acknowledgment

The authors would like to acknowledge the support of King Fahd University of Petroleum and Minerals on this work.

References

1. R. Moeller, Thermal Processing Particularly Significant in Developing Corrosion Resistant Alloys for Sour Gas Wells, *Ind. Heat.*, Vol 56 (No. 12), 1989, p 29-30
2. P. Shewmon, Y.L. Shen, C.H. Shen, and M. Meshii, Analysis of Diffusion Controlled Release of Hydrogen from Nickel and Inconel 600, *Acta Metall.*, Vol 37 (No. 7), 1989, p 1913-1921
3. W.T. Tsai, Z.H. Lee, and J.T. Lee, Electrochemical and SCC Behavior of Inconel 600 (UNS NO 6600) in Thiosulfate Solution, *Corrosion*, Vol 45 (No. 11), 1989, p 883-884
4. D.A. Jones, Localized Corrosion, *Corrosion Processes*, R.N. Parkins, Ed., Applied Science Publishers, 1982
5. J.F. Sykes, A.K. Agrawal, and W.E. Berry, Pitting Corrosion of Alloy 600 Steam Generator Tubing: Results of a Laboratory Scoping Study, Final Report EPRI-NP-3905, EPRI, Feb 1985
6. P.J. King and D.D. Doutovich, Pitting Corrosion of Nuclear Steam Generator Materials, *Nucl. Technol. ANS*, Vol 55, 1981, p 196-201
7. H.S. Isoacs, Localized Electrochemical Corrosion of Nickel Based Alloys, Final Report EPRI-NP-4754, EPRI, Sept 1986
8. J.T. Ho and G.P. Yu, Pitting Corrosion of Inconel 600 in Chloride and Thiosulfate Anion Solutions at Low Temperatures, *Corrosion*, Vol 48 (No. 2), 1992, p 147-158
9. D. Choi and G.S. Was, Development of a Pit Growth Resistance Parameter for the Study of Pit Growth in Alloy 600, *Corrosion*, Vol 48 (No. 4), 1992, p 292-305